

# Earth's Future

## RESEARCH ARTICLE

10.1029/2025EF007008

# Rapid Loss of Terrestrial Ecosystem Multifunctionality in China on a Century Scale



### Key Points:

- Ecosystem multifunctionality was primarily lower in northwestern China, and higher in northeastern China and southeastern Tibetan Plateau
- Ecosystem multifunctionality varied significantly across climatic zones, driven mainly by climate and topography
- More than 66% of ecosystem multifunctionality is projected to experience degradation by 2100 under future climate scenarios

### Supporting Information:

Supporting Information may be found in the online version of this article.

### Correspondence to:

J. Sun,  
[sunjian@itpcas.ac.cn](mailto:sunjian@itpcas.ac.cn)

### Citation:

He, W., Sun, J., Di, B., & Peñuelas, J. (2026). Rapid loss of terrestrial ecosystem multifunctionality in China on a century scale. *Earth's Future*, 14, e2025EF007008. <https://doi.org/10.1029/2025EF007008>

Received 30 JUL 2025

Accepted 8 FEB 2026

### Author Contributions:

**Conceptualization:** Wen He, Jian Sun  
**Data curation:** Wen He  
**Formal analysis:** Wen He  
**Funding acquisition:** Jian Sun, Baofeng Di, Josep Peñuelas  
**Methodology:** Wen He, Jian Sun, Baofeng Di, Josep Peñuelas  
**Project administration:** Jian Sun  
**Resources:** Wen He, Baofeng Di, Josep Peñuelas  
**Software:** Wen He  
**Supervision:** Jian Sun  
**Validation:** Wen He  
**Visualization:** Wen He  
**Writing – original draft:** Wen He, Jian Sun, Baofeng Di  
**Writing – review & editing:** Wen He, Jian Sun, Baofeng Di, Josep Peñuelas

© 2026. The Author(s).

This is an open access article under the terms of the [Creative Commons Attribution License](https://creativecommons.org/licenses/by/4.0/), which permits use, distribution and reproduction in any medium, provided the original work is properly cited.

Wen He<sup>1,2</sup> , Jian Sun<sup>2,3</sup> , Baofeng Di<sup>1</sup> , and Josep Peñuelas<sup>4,5</sup> 

<sup>1</sup>Institute for Disaster Management and Reconstruction, Sichuan University-HongKong Polytechnic University, Chengdu, China, <sup>2</sup>State Key Laboratory of Tibetan Plateau Earth System, Environment and Resources (TPESER), Institute of Tibetan Plateau Research, Chinese Academy of Sciences, Beijing, China, <sup>3</sup>Yunnan Key Laboratory of Plateau Geographical Processes and Environmental Change, Faculty of Geography, Yunnan Normal University, Kunming, China, <sup>4</sup>CREAF, Barcelona, Spain, <sup>5</sup>CSIC, Global Ecology Unit CREAM-CSIC-UAB, Barcelona, Spain

**Abstract** Ecosystem multifunctionality (EMF) is a crucial factor in protecting biodiversity and regulating climate dynamics. However, the global and regional dynamics of EMF are currently limited to field experiments, resulting in an incomplete understanding of the spatial patterns and driving mechanisms of EMF. We focused on biogeochemical cycles to quantify the spatiotemporal dynamics of EMF in China and determine the impact of environmental factors on EMF. Our findings indicate that climate and topography are the primary drivers of EMF. More importantly, over 66% of the study area is expected to experience a decline in EMF by the end of the twenty-first century across various future climate scenarios. Under high-emission scenarios in particular, EMF could be on an unsustainable trajectory, putting increased pressure on terrestrial ecosystems and exacerbating their degradation. These results highlight that more robust policies need to be designed to mitigate ecosystem degradation triggered by climate change.

**Plain Language Summary** Understanding ecosystem multifunctionality (EMF) is crucial for conserving biodiversity and regulating climate. However, the geographic patterns and environmental drivers of EMF on a large scale remain unclear. Our evaluation of EMF dynamics across China revealed significant geographic patterns and identified climate and topography as the primary drivers. Projections indicate that over 66% of China could experience declines in EMF by the end of the century, particularly under high-emission scenarios. These findings underscore the urgent need for stronger policies to prevent widespread ecosystem degradation.

## 1. Introduction

Terrestrial ecosystems provide a range of functions that support human productive activities, including biomass production, energy cycling, and information transfer (Wagg et al., 2014; Zavaleta et al., 2010). Nevertheless, dramatic climate change is altering the functions of terrestrial ecosystems at unprecedented rates, leading to a rapid decline in ecosystem stability and water shortages, accelerated desertification, and continuous biodiversity loss (Cardinale et al., 2012; Gamfeldt et al., 2008; Song et al., 2020; van der Plas, 2019). Global warming is indisputable and likely to reach or exceed 1.5°C in the near future if sustainable practices are not implemented, which would have a remarkable impact on our survival and development (Masson-Delmotte et al., 2021; Oliver et al., 2015; Schuur et al., 2015). Land use is also strongly reducing ecosystem functions such as vegetation productivity (Sun, Fu, et al., 2021; Sun, Liang, et al., 2021) and litter decomposition (Both et al., 2017). Global plans and initiatives to protect the environment, reduce negative influences on natural resources, and promote ecosystem sustainability are currently being implemented, including the Convention on Biological Diversity, the United Nations Convention to Combat Desertification, and the United Nations Framework Convention on Climate Change. Quantifying and monitoring ecosystem functions have become the keystone for assessing ecosystem sustainability as these actions have advanced (Carpenter et al., 2009). Consequently, it is of great importance to accurately understand the comprehensive capacity of multiple ecosystem functions (ecosystem multifunctionality, EMF) for regional sustainable management (Hector & Bagchi, 2007; Manning et al., 2018; Oliver et al., 2015).

Previous reports have mostly focused on EMF changes and driving forces (Jing et al., 2015; Wang, Liu, et al., 2022; Wang, Sun, et al., 2022). The relationship between biodiversity and EMF has been explored in grassland, dryland, and forest ecosystems (Jing et al., 2015; Maestre et al., 2012; van der Plas et al., 2016).

Numerous in situ experiments have found that biodiversity can increase EMF, with varying dynamics depending on the geographic units (Bradford et al., 2014; Delgado-Baquerizo, Maestre, Eldridge, et al., 2016; Delgado-Baquerizo, Maestre, Reich, et al., 2016; Gamfeldt & Roger, 2017; Jing et al., 2020). Habitat conditions also play a crucial role in regulating EMF across different ecosystems. Specifically, environmental changes within climatic zones may impact EMF more strongly than biodiversity (Fry et al., 2016; van der Plas, 2019; Wang et al., 2023; Xu et al., 2021; Zirbel et al., 2019). For example, drought can directly affect EMF via altering carbon, nitrogen and phosphorus cycles in arid regions (An et al., 2019), whereas climate can indirectly regulate EMF by affecting biodiversity across spatial scales, as demonstrated in field experiments (Fry et al., 2016; Jing et al., 2015; Maestre et al., 2012). In short, the interaction between biological and abiotic factors determines the provision and spatiotemporal variation of EMF. However, while meta-analyses synthesize EMF findings across multiple sites, they remain constrained by spatial discontinuity and inconsistent methods (Garland et al., 2021; Jing et al., 2015). By contrast, remote sensing products are characterized by ready availability and extensive spatial coverage, which is essential for capturing spatial patterns and drivers of EMF across climatic gradients (Zhou et al., 2025).

We hypothesized that geographic differences in EMF would be regulated primarily by regional climate dynamics. To test this hypothesis, we evaluated the spatial distribution of terrestrial EMF in China and explored the effects of topography, climate, soil properties, and plant biodiversity on EMF across eight climatic zones. These zones include the plateau climatic zone (PC), the northern temperate zone (NT), the mid-temperate zone (MT), the southwestern temperate zone (SWT), the southeastern temperate zone (SET), the northern subtropical zone (NST), the mid-subtropical zone (MST), and the southern subtropical zone (SST). Additionally, we predicted future EMF variations using a random forest algorithm to determine the effects of various socioeconomic pathways and global warming. We excluded lake, ice, and snow ecosystems due to the lack of comprehensive spatial data on their ecosystem functions.

## 2. Materials and Methods

### 2.1. Division of Climatic Zones

We divided the study area into eight zones according to the climatic gradients defined by China's National Meteorological Administration and topographical features: PC, NT, MT, SWT, SET, NST, MST, and SST (Figure 1a). PC, MT, and SWT are in arid and semi-arid regions, consisting primarily of grassland and desert. SET is situated in a sub-humid region, comprising primarily forest and grassland ecosystems. NT, NST, MST, and SST are located in humid regions where forests dominate the landscape. PC has an average altitude of over 4,000 m, making it the highest zone, and it exhibits unique alpine climatic characteristics (Sun et al., 2020).

### 2.2. Ecosystem Functions

Soil physical and chemical properties, vegetation, and microorganisms are essential indicators for quantifying EMF. We selected 14 variables: soil available nitrogen (SAN), soil available phosphorus (SAP), soil total nitrogen (STN), soil total phosphorus (STP), soil organic matter (SOM), soil microbial biomass carbon (SMBC), soil microbial biomass nitrogen (SMBN), soil microbial biomass phosphorus (SMBP), aboveground biomass carbon (ABC), belowground biomass carbon (BBC), vegetation leaf nitrogen (VLN), vegetation leaf phosphorus (VLP), vegetation root nitrogen (VRN), and vegetation root phosphorus (VRP), according to previous research (Garland et al., 2021; Meyer et al., 2018).

SAN, SAP, STN, STP, and SOM were obtained from the National Tibetan Plateau Data Center (Shangguan & Dai, 2021) with a resolution of 30" and a depth of 0.045 m, while SMBC, SMBN, and SMBP were acquired from the Zenodo platform (Gao et al., 2022) with a resolution of 30" and a depth of 0.30 m. ABC and BBC were also obtained from the Oak Ridge National Laboratory Distributed Active Archive Center (Spawn & Gibbs, 2020) with a spatial resolution of 10". Bilinear interpolation is suited for continuous variables like biomass as it preserves spatial gradients by weighting neighboring pixels (Bovik, 2009). The above-mentioned data sets were resampled to a resolution of 30" using bilinear interpolation in R software version 4.0.0 (R Core Team, 2020). Validation against a mass-conserving baseline (area-weighted mean aggregation) confirmed small mass deviation (<0.001% for ABC and BBC), high spatial correlation (ABC:  $r = 0.997$ ; BBC:  $r = 0.996$ ) and low root mean square error (ABC: RMSE = 14.34 Mg C ha<sup>-1</sup>; BBC: RMSE = 5.47 Mg C ha<sup>-1</sup>).

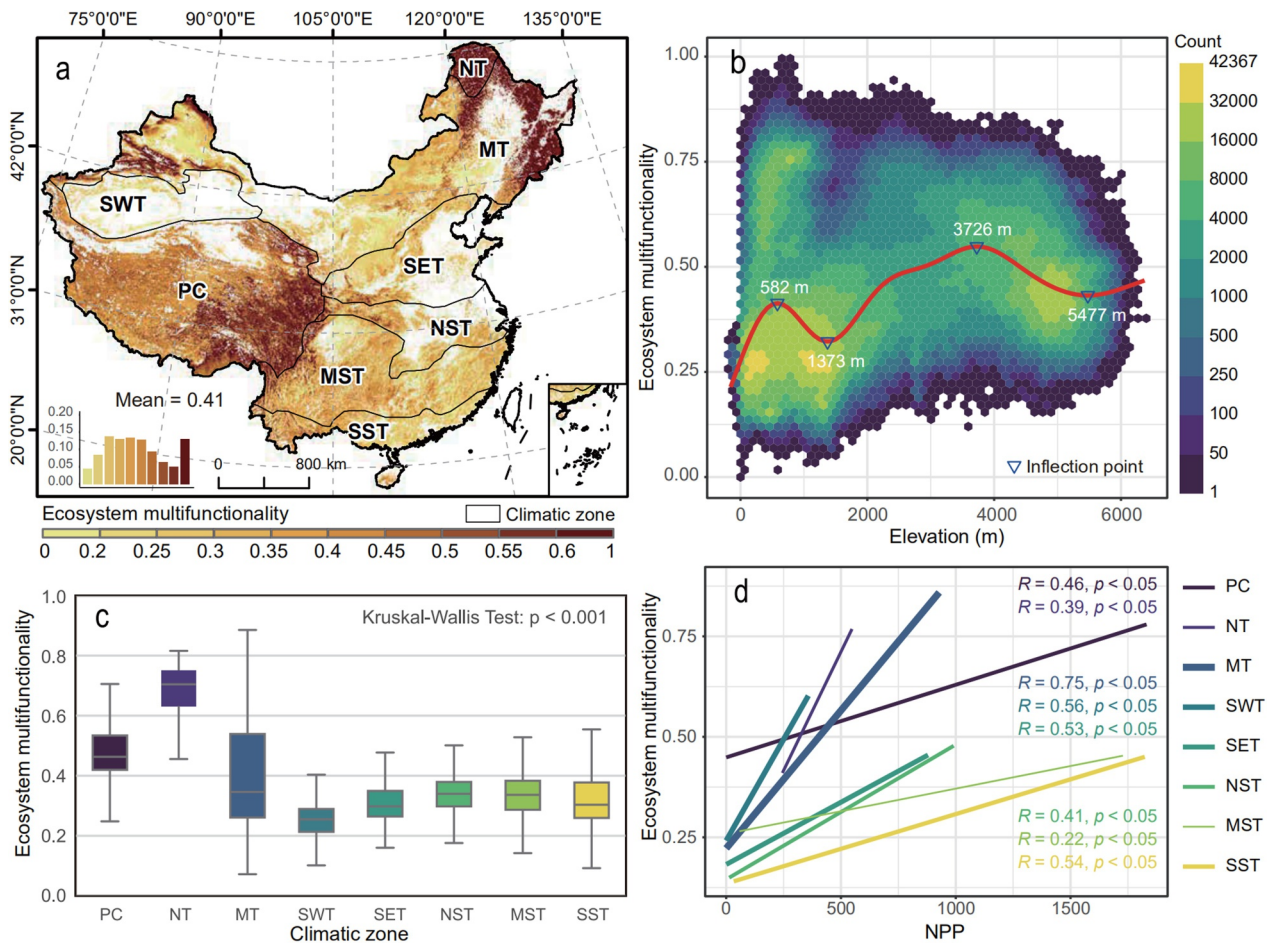


**Figure 1.** Spatial pattern and difference of ecosystem multifunctionality. (a) Spatial patterns of ecosystem multifunctionality. (b) Elevation-dependent change in ecosystem multifunctionality. (c) Kruskal-Wallis analysis of ecosystem multifunctionality based on climatic zones. (d) Fitted linear relationships between NPP and ecosystem multifunctionality based on climatic zones. Climatic zones are as follows: plateau climatic zone (PC), northern temperate zone (NT), mid-temperate zone (MT), southwestern temperate zone (SWT), southeastern temperate zone (SET), northern subtropical zone (NST), mid-subtropical zone (MST), and southern subtropical zone (SST).

Vegetation traits (VLN, VLP, VRN, and VRP) were obtained from the Dryad digital repository (Zhang et al., 2021) with a resolution of 30". In detail, SAN, SAP, STN, and STP are essential nutrients for plant growth (Jing et al., 2015). SOM is associated with soil fertility and nutrient cycling, whereas SMBC, SMBN and SMBP are associated with the sequestration of soil carbon and nitrogen (Maestre et al., 2012). ABC and BBC can represent material productivity. In summary, these 14 indicators provide a crucial foundation for EMF assessment (Isbell et al., 2011).

### 2.3. Environmental Factors

#### 2.3.1. Bioclimate

Regional climate changes determine the structure and function of various ecosystems (Delgado-Baquerizo, Maestre, Eldridge, et al., 2016; Delgado-Baquerizo, Maestre, Reich, et al., 2016; Jing et al., 2015). Considering multidimensional bioclimatic factors and examining their impact on the dynamics of ecosystem function is of particular significance (Garcia et al., 2014). To ensure consistency in assessing climate change impacts, we used 19 bioclimatic indicators in both historical and future periods (Table S1 in Supporting Information S1). Current bioclimatic data are available in Fick and Hijmans (2017). Future bioclimatic data are available at [https://www.worldclim.org/data/cmip6/cmip6\\_clim30s.html](https://www.worldclim.org/data/cmip6/cmip6_clim30s.html). Future bioclimates were produced using an ensemble of 11 global climate models: ACCESS-CM2, CMCC-ESM2, EC-Earth3-Veg, GISS-E2-1-G,

INM-CM5-0, IPSL-CM6A-LR, MIROC6, MPI-ESM1-2-HR, MRI-ESM2-0, UKESM1-0-LL, and BCC-CSM2-MR. The data from these models were averaged to project future bioclimates. The projections are divided into the following periods: 2021–2040, 2041–2060, 2061–2080, and 2081–2100. Each period corresponds to the four Shared Socioeconomic Pathways (SSPs): SSP126, SSP245, SSP370, and SSP585. These pathways represent sustainability, middle of the road, regional rivalry, and fossil-fueled development, respectively (Riahi et al., 2017).

### 2.3.2. Topography

Topographic effects can alter general climate patterns (Wang et al., 2023). A digital elevation model (DEM) was obtained from the SRTM 90 m DEM digital elevation database (Jarvis et al., 2008) with a spatial resolution of 30", which was generated according to the most recent data resampling of the Shuttle Radar Topography Mission (SRTM) V4.1 data. Other topographic factors, such as slope and aspect, were extracted from the DEM data using R software version 4.0.0 (R Core Team, 2020).

### 2.3.3. Soil Abiotic Properties

Soil abiotic properties are important indicators for identifying the mechanisms driving EMF (Garland et al., 2021), which include bulk density, clay concentration, porosity, and pH. They were obtained from the National Tibetan Plateau Data Center (Shangguan & Dai, 2021) with a resolution of 30" and a depth of 0.045 m. Moreover, soil moisture content was downloaded from the Zenodo platform (Zhang et al., 2022) with a spatial resolution of 30".

### 2.3.4. Plant Biodiversity

To quantify the relationship between biodiversity and EMF, we used a global species richness data set with a resolution of 30", obtained from the German Centre for Integrative Biodiversity Research (Sabatini et al., 2022).

## 2.4. Net Primary Productivity

Net primary productivity (NPP) is a crucial indicator of the health and sustainable development of terrestrial ecosystems (Field et al., 1998). Thus, we used NPP to evaluate EMF performance. NPP was derived from the MOD17A3HGF V6 data set (Running & Zhao, 2021) with a horizontal resolution of 15" and an annual interval. Subsequently, the data were resampled to 30" using bilinear interpolation in R software version 4.0.0 (R Core Team, 2020), thereby maintaining the same spatial resolution as other products.

## 2.5. Assessing EMF

Several methods have been proposed for calculating EMF, including the single-function method (Jing et al., 2015), the turnover method (Hector & Bagchi, 2007), the averaging method (Jing et al., 2015; Wagg et al., 2014), the single-threshold method (Gamfeldt et al., 2008; Zavaleta et al., 2010), the multi-threshold method (Bradford et al., 2014), and the multivariate-model method (Dooley et al., 2015). Considering applicability for large-scale assessment, three complementary methods were selected to calculate EMF: (a) the averaging method, which provides an integrated measure of overall function via averaging all ecosystem functions; (b) the principal-component method, which identifies key dimensions of covariance among ecosystem functions; and (c) the multi-threshold approach, which determines areas that meet critical benchmarks for multiple functions simultaneously. These three methods have different characteristics, to avoid being limited by any single method, we averaged their results to obtain a more comprehensive assessment of EMF.

### 2.5.1. Averaging Method

The averaging method is the most extensive and simple approach for quantifying EMF. Specifically, each ecosystem function was first standardized, and then EMF was obtained by averaging the ecosystem functions at a spatial pixel scale. The averaging method is defined as follows:

$$\text{EMF}_{\text{average}} = \frac{1}{F} \sum_{i=1}^F g(r_i(f_i)) \quad (1)$$

where  $F$  is the number of ecosystem functions,  $f_i$  is the value of ecosystem function  $i$ ,  $r_i$  is a mathematical function that converts values to positive values, and  $g$  is a standardized function.

All ecosystem functions first needed to be standardized to ensure that they were on the same scale. We used the method of converting maximum values to standardize the ecosystem functions:

$$N_{\max} = \frac{EF_i}{MAX_{5\%}} \quad (2)$$

where  $EF_i$  is the  $i$ th value of an ecosystem function, and  $MAX_{5\%}$  is the average of the highest 5% of the ecosystem function rankings.  $MAX_{5\%}$  was calculated using the “*xarray*” and “*gdal*” packages in the Python software version 3.13.5 (Python Software Foundation, 2023).

### 2.5.2. Principal-Component Method

The principal-component method is a common form of multivariate analysis that primarily utilizes the concept of dimensionality reduction to extract important information from multidimensional data (Abdi & Williams, 2010). These derived variables are called principal components (PCs). The obtained PCs are independent and can represent most of the information in the original data set. These PCs are then weighted by contribution rates and summed to calculate EMF. The formula is listed below:

$$EMF_{PCA} = \sum_{i=1}^n \alpha_i PC_i \quad (3)$$

where  $PC_i$  is the principal component  $i$ ,  $\alpha_i$  is the contribution rate corresponding to PC  $i$  and  $n$  is the number of PCs selected. The principal components are selected with a cumulative contribution rate of at least 75% (He et al., 2020).

### 2.5.3. Multi-Threshold Method

The multi-threshold method is a common approach to calculating EMF. We implemented this approach in three steps: (a) calculating quantile-based thresholds at 10% intervals from 10% to 90% of each function's maximum value (defined as the 95th percentile value); (b) converting function values to binary indicators (1 if  $\geq$  threshold, 0 otherwise) at each threshold level; and (c) summing these binary indicators to compute EMF. The final integrated EMF was computed by averaging the results obtained at each threshold level using the R “*terra*” package.

Three kinds of EMF grid data were obtained using the above methods. We averaged grids on a pixel scale, considering the characteristics of each method, to produce the “mean” product. Prior to integration, the three EMFs were standardized to a common 0–1 scale using min-max normalization to ensure comparability across their different measurement scales.

### 2.6. Spatial Similarity of EMF

The comparison map profile (CMP) method was selected for analyzing spatial similarities and consistencies in the EMF grid data. The principle of CMP is to analyze spatial consistency by setting the size of the moving window (Gauchere et al., 2008). The cross-correlation coefficient (CC) and absolute distance (AD) were utilized to assess the degrees of similarity and consistency. The absolute distance was calculated as follows:

$$AD = \text{abs}(\bar{x} - \bar{y}) \quad (4)$$

where  $\bar{x}$  and  $\bar{y}$  represent the average pixel values in the moving windows applied to the first and second remote sensing images, respectively; and  $\text{abs}()$  is a function that converts a value to an absolute value. The lower the AD, the higher the similarity between the two images. Cross-correlation represents the similarity or difference of two images in the gradient direction, calculated as follows:

$$CC = \frac{1}{N^2} \sum_{i=1}^N \sum_{j=1}^N \frac{(x_{ij} - \bar{x})(y_{ij} - \bar{y})}{\sigma_x \sigma_y} \quad (5)$$

$$\sigma_x^2 = \frac{1}{N^2 - 1} \sum_{i=1}^N \sum_{j=1}^N (x_{ij} - \bar{x})^2 \quad (6)$$

where  $x_{ij}$  and  $y_{ij}$  represent the pixel values of row  $i$  and column  $j$  in the moving window of the two images  $x$  and  $y$ , respectively,  $N$  is the total number of pixels in each moving window, and  $\sigma_x$  and  $\sigma_y$  are the standard deviations of the pixel values in the two comparison moving windows. The maps of the AD and CC values were calculated 20 times, with the window size increasing from  $2 \times 2$  pixels to  $21 \times 21$  pixels (Gaucherel et al., 2008; Li et al., 2018). The similarity analysis was performed using CMP software version 2.1 (Gaucherel et al., 2018).

### 2.7. EMF Differences

To assess the differences in EMF across different environments, the Kruskal-Wallis test (Kruskal & Wallis, 1952) was employed. This non-parametric approach is particularly advantageous for ecological data, which often does not adhere to the assumptions of a normal distribution. It effectively handles samples of different sizes and variances, which is a common occurrence in multidisciplinary environmental research. The Kruskal-Wallis test was performed using the “scipy.stats” package in Python software version 3.13.5 (Python Software Foundation, 2023).

### 2.8. Drivers of EMF

Pearson correlation coefficients were determined using the “PerformanceAnalytics” package in R software version 4.0.0 (R Core Team, 2020) to confirm the degree of correlation between EMF and the environmental variables (topography, climate, soil abiotic factors, and biodiversity). For each climatic zone, a principal-component analysis was conducted on the following three variable categories: topography, climate, and soil abiotic factors. The first two principal components from each category were retained to create composite environmental factors. To address multicollinearity, variables with variance inflation factors (VIF)  $< 5$  were selected for inclusion in subsequent analyses (Hu et al., 2021; Jing et al., 2015). Then, separate structural equation models (SEMs) were constructed for each climatic zone to quantify direct and indirect pathways influencing EMF. The assessment of model fitness was conducted by the Akaike Information Criterion (AIC), Fisher's  $C$  statistics, and the associated  $P$ -values. The “piecewiseSEM” package in R software version 4.0.0 (R Core Team, 2020) facilitated the construction of models and the decomposition of effects, enabling the partitioning of total effects into direct and indirect components.

### 2.9. Predicting Dynamics of EMF

The random forest algorithm is a machine-learning method based on classification and regression trees. It is considered to be one of the most accurate prediction methods in regression modeling (Cutler et al., 2007). Random forest algorithms have been widely applied in the field of environmental remote sensing, including land-cover classification, and environmental and water resource management (Booker & Snelder, 2012). Many environmental variables typically influence EMF when mapping future spatial patterns, and the relationship between these variables is complex. For the prediction of future EMF, we made two key assumptions: (a) non-climatic variables (including soil abiotic properties, topography, and biodiversity) would remain constant at present-day levels, and (b) the observed relationships between EMF and environmental drivers would persist under future climate conditions. To this end, a random forest regression algorithm and future bioclimate data were utilized to predict the spatial pattern of EMF under future scenarios. Specifically, the bioclimatic data was divided into training and test sets at a ratio of 4:1 from the different climatic zones. The training-test split was implemented through stratified random sampling by climatic zone using the “caret” package in R software version 4.0.0 (R Core Team, 2020), which maintains ecological representativeness within each climatic zone while guaranteeing data independence between the training and test sets. Subsequently, a random-forest regression model comprising 500 decision trees was established for the purpose of training. Finally, the model was employed to predict the spatial pattern of the EMF under different climatic zones. The random-forest regression was

developed via the “*randomForest*” package in R software version 4.0.0 (R Core Team, 2020). The reliability of the predicted results was ensured by adopting the correlation coefficient ( $r$ ) and root mean square error (RMSE).

### 3. Results

#### 3.1. EMF Across China

We evaluated three EMF products, considering the differences in the methods for quantifying EMF (see Methods) (Figure S1 in Supporting Information S1). We further calculated the spatially explicit indices CC and AD at multiple scales to examine spatial similarities between the three results using the CMP method. Both  $CC > 0.85$  and  $AD < 0.14$  indicated that the three EMFs had highly consistent and similar spatial structures and values (Figure S2 in Supporting Information S1). Nevertheless, these methods were still spatially heterogeneous in certain areas. To reduce spatial variation and uncertainty in these methods, the “mean” EMF product was calculated (Figure 1a), which notably improved after averaging (Figures S2d–S2f and S2j–S2l in Supporting Information S1). Specifically, the “mean” EMF product showed superior spatial agreement with the individual methods, as evidenced by higher consistency ( $CC > 0.93$ ) and lower discrepancy ( $AD < 0.08$ ), thereby effectively reducing extreme discrepancies among methods.

The spatial pattern of EMF in China presented a heterogeneous geographical pattern. Specifically, the average EMF in China was 0.41, with approximately 56% of the study area below this average value (Figure 1a). It was demonstrated that regions in northeastern China, the southeastern Tibetan Plateau, the Tianshan Mountains, and the Altai Mountains experienced high EMF, while the low EMF was observed in the Taklimakan Desert and Loess Plateau. Among the various land use types, EMF was found to be highest in forests, followed by grasslands, and barren lands (Figure S3 in Supporting Information S1). Furthermore, EMF exhibited distinct topographic gradient characteristics, with four elevation thresholds identified at 582 m, 1,373 m, 3,726 m, and 5,477 m (Figure 1b). Interestingly, EMF increased to reach its maximum at the 3,726-m contour lines, which were primarily located on the edge of the Tibetan Plateau (Figure S4 in Supporting Information S1).

A Kruskal-Wallis analysis revealed that EMF differed significantly among different climatic zones ( $P < 0.001$ , Figure 1c), suggesting that climate may influence the spatial distribution of EMF. EMF was found to be highest in NT, followed by PC, primarily in regions with harsh cold climates and high latitudes. EMF was lowest in SWT, which contains the Taklimakan Desert. NPP and EMF were significantly positively correlated across climatic zones (Figure 1d). The correlation between NPP and EMF was the strongest in MT, with a coefficient of 0.75.

#### 3.2. Links of Environmental Factors With EMF

Environmental factors play important roles in determining EMF. We first assessed the relationships between bioclimatic factors and EMF (Figure 2). The findings revealed that most temperature factors (>82%) exhibited a significant inhibitory effect ( $P < 0.05$ ) on EMF across all climatic zones, with the exception of PC. In SWT, the negative impact of most temperature factors on EMF was more substantial. Temperature fluctuations (i.e., mean diurnal range, isothermality, and annual range of temperature) harmed EMF in PC. Conversely, mean diurnal range in temperature and isothermality exhibited significant positive effects ( $P < 0.05$ ) on EMF in tropical zones (NST, MST, and SST). In NT, the seasonality and annual range of temperature were found to have a significant positive impact ( $P < 0.05$ ) on EMF. The majority of precipitation factors demonstrated significant positive effects ( $P < 0.05$ ) on EMF in PC, MT, SWT, and SET, while remarkable negative effects ( $P < 0.05$ ) were observed in NST, MST, and SST. The study found that precipitation seasonality exhibited a strong positive effect ( $P < 0.05$ ) on EMF in tropical zones (NST, MST, and SST), but demonstrated a weaker negative or neutral effect in polar and temperate zones.

Furthermore, linkages among the abiotic properties of soil, topographic factors, biodiversity, and EMF were explored in Figure 2. Notably, elevated soil bulk density tended to impair EMF across most climatic zones. In contrast, soil pH showed divergent effects. Higher pH enhanced EMF in NST, MST, and SST, whereas lower values were beneficial in other zones. Regarding topography, slope exhibited a positive influence on EMF, albeit strictly within an optimal range. Most strikingly, biodiversity displayed contrasting relationships with EMF across regions, with strong positive correlations in PC, MT, and SWT but negative associations in NST, MST, and SST.

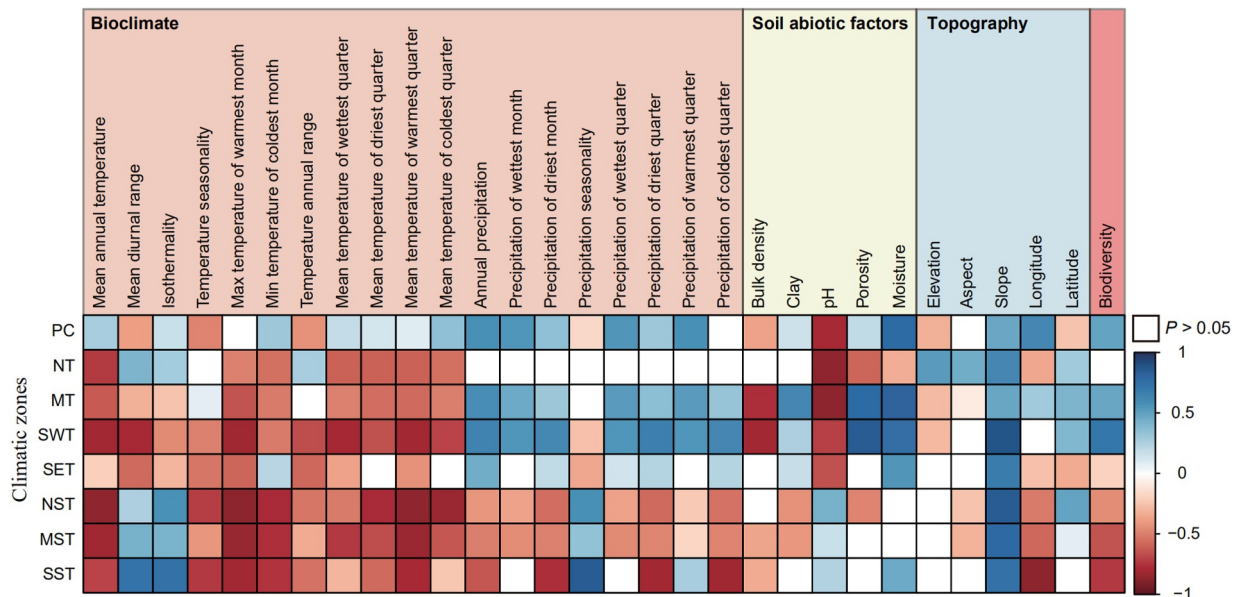


**Figure 2.** Relationship between environmental factors and ecosystem multifunctionality in the climatic zones. Heatmap showed significant correlations ( $P < 0.05$ ). The color of the square denoted a positive (blue) or negative (red) correlation, and color intensity indicated the strength of the correlation. Environmental factors were grouped into four categories (colored backgrounds of the column names): bioclimate variables, soil abiotic properties, topography, and biodiversity. Climatic zones are as follows: plateau climatic zone (PC), northern temperate zone (NT), mid-temperate zone (MT), southwestern temperate zone (SWT), southeastern temperate zone (SET), northern subtropical zone (NST), mid-subtropical zone (MST) and southern subtropical zone (SST). The rows of the heatmap represented EMF in different climatic zones, while the columns represented environmental factors.

We then constructed SEMs to assess the relative strengths of direct and indirect relationships among bioclimate variables, soil abiotic properties, topography, biodiversity and EMF among different climatic zones. The results of the SEMs demonstrated an excellent fit ( $1.35 < Fisher's C < 9.54$ ,  $P > 0.05$ , Figure S5 in Supporting Information S1) and the standardized total effects revealed bioclimate and topography factors as the predominant regulators of EMF across climatic zones (Figure 3). Notably, it was found that soil abiotic factors had the largest positive and integrated effects (standardized total effect = 0.82) on EMF in PC, followed by topography and bioclimate. In most climatic zones, bioclimate exerted substantial direct effects on EMF, particularly in the NST, MST, and SWT. Furthermore, the bioclimate indirectly enhanced EMF by mediating soil abiotic properties. The effects of topography were primarily indirect, operating through climate modulation. Biodiversity showed inconsistent effects, with a significant positive effect on PC (standardized total effect = 0.22) and significant negative impacts in MT (standardized total effect =  $-0.29$ ) and NT (standardized total effect =  $-0.16$ ).

### 3.3. EMF Change Under Future Climatic Scenarios

Bioclimate and topography are the main driving factors of EMF across climatic zones. Topography in most areas may have been less affected by biological and abiotic factors over long timescales. To predict future EMF, it was hypothesized that non-climate variables would remain unchanged at the current level. We predicted changes in EMF according to quantitative estimates from the SSPs, namely SSP126, SSP245, SSP370, and SSP585 (Figure 4), until the end of the century. The random-forest model demonstrated robust and accurate performance ( $R > 0.88$ ,  $RMSE < 0.04$ ), as evidenced by validation analysis (Figure S6 in Supporting Information S1). Our estimates indicated that, under the SSP126, SSP245, SSP370, and SSP585 scenarios, 66.20%, 67.79%, 70.18%, and 69.69% of the study area, respectively, would be degraded by the year 2100. The most severely degraded areas were mainly located in northeast and southern China, and the western Tibetan Plateau, with the highest degree of degradation occurring in northeastern China. Conversely, increases in EMF were predominantly projected in the eastern Tibetan Plateau and the Loess Plateau, indicating potential heterogeneity in the impacts of climate change. Temporal analysis revealed a consistent and progressive decline in EMF across all scenarios (Figure 5). Initial periods demonstrated moderate losses, with a range of  $-4.48\%$  to  $-5.02\%$ . However, by the end of the century, there was a marked intensification in the reduction of EMF, reaching  $-5.68\%$  (SSP126),  $-7.74\%$  (SSP245),  $-9.71\%$  (SSP370), and  $-10.33\%$  (SSP585).

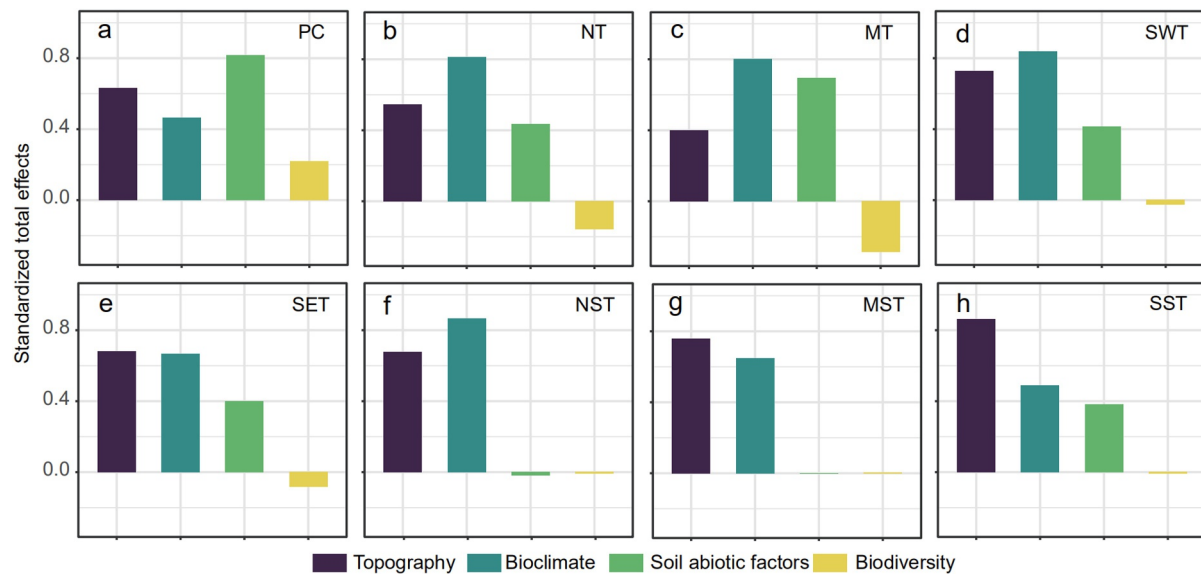


**Figure 3.** Standardized total effects of environmental factors on ecosystem multifunctionality in the climatic zones. (a) Plateau climatic zone (PC). (b) Northern temperate zone (NT). (c) Mid-temperate zone (MT). (d) Southwestern temperate zone (SWT). (e) Southeastern temperate zone (SET). (f) Northern subtropical zone (NST). (g) Mid-subtropical zone (MST). (h) Southern subtropical zone (SST). The standardized total effect represented the sum of direct and indirect standardized path coefficients derived from structural equation models. Positive values indicated enhancing effects on ecosystem multifunctionality, while negative values indicated suppressing effects. Environmental factors were categorized into four groups: bioclimate variables, soil abiotic properties, topography, and biodiversity.

The tendencies of EMF revealed that only the PC exhibited EMF increases. However, all other zones showed a gradual decline in the different scenarios, particularly in the high-emission scenario (Figure 6). By the year 2100, under SSP585, MT exhibited the most pronounced decline (22.97%, 0.092), followed by NT (9.52%, 0.066). The sustainable development pathway (SSP126) has been confirmed to facilitate EMF stabilization during the latter half of the present century, while accelerated declines were demonstrated in SSP585. This discrepancy underscores the imperative for the adoption of sustainable development pathways.

## 4. Discussion

### 4.1. Nondeterminacy and Size of EMF

EMF is essential for evaluating the health, stability, and sustainability of an ecosystem (Garland et al., 2021; Mastrangelo et al., 2014). Nevertheless, EMF assessment is uncertain owing to variability in indicator selection and methodological differences, both of which reduce the reliability and comparability of EMF assessment (Jing et al., 2015; Maestre et al., 2012). A primary challenge in EMF assessment lies in the selection of appropriate ecosystem functions. While studies have employed anywhere from 2 to 82 indicators, this wide variability introduces uncertainty, as different function sets may lead to divergent conclusions about ecosystem performance (Garland et al., 2021). The choice of indicators should reflect specific ecosystem processes (e.g., nutrient cycling, productivity, or decomposition) rather than abiotic drivers (e.g., soil pH, moisture, or bulk density), which are environmental constraints rather than true function outputs (Garland et al., 2021; Maestre et al., 2012; Meyer et al., 2018). Despite this, the accurate quantification of EMF remains challenging due to trade-offs or redundancies among ecosystem functions (Bradford et al., 2014; Byrnes et al., 2014; Lavorel & Grigulis, 2012). Meanwhile, the temporal discrepancy between ecosystem function data sets must be considered. For instance, soil chemistry data, microbial biomass data, biomass carbon data, and vegetation traits span different decades. While these data sets represent the most comprehensive and authoritative sources available for our study region, it is recognized that temporal discrepancies may introduce some uncertainty in our integrated analysis. Furthermore, the diverse approaches to assessing EMF pose considerable limitations for researchers, hindering the comparison of results across studies. Given these difficulties, we adopted a multi-method approach, using the “mean” EMF across different quantification techniques to reduce bias and enhance robustness at the spatial pixel scale (Figure S2 in Supporting Information S1).

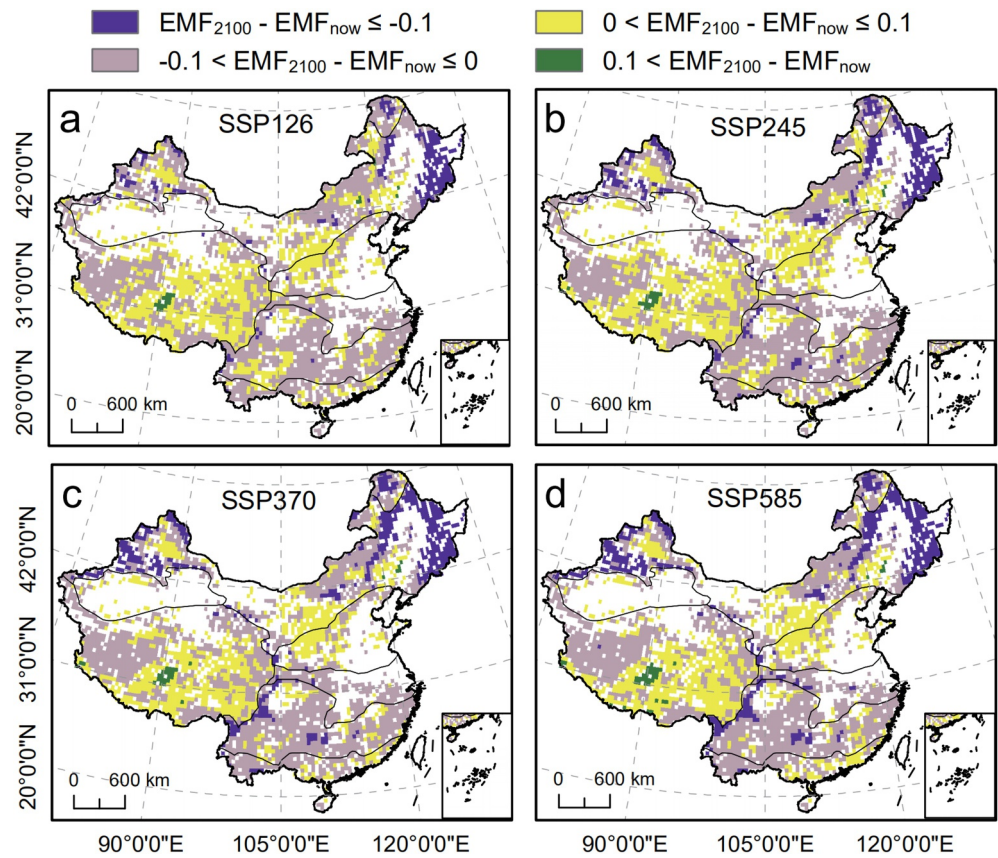


**Figure 4.** Magnitude of changes in ecosystem multifunctionality between the present and 2100 under various climatic scenarios. (a) SSP126 (sustainability). (b) SSP245 (middle of the road). (c) SSP370 (regional rivalry). (d) SSP585 (fossil-fueled development).

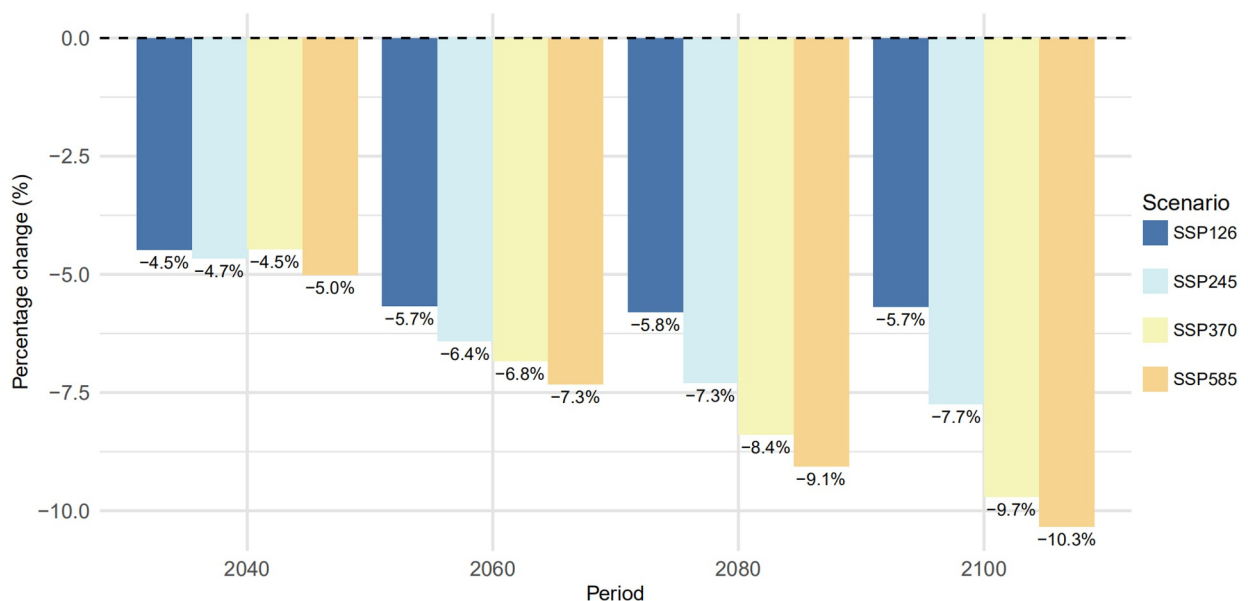


**Figure 5.** Percentage change of ecosystem multifunctionality in China under different climatic scenarios. The bar plot shows percentage changes of ecosystem multifunctionality relative to baseline conditions for four future periods (2040, 2060, 2080, 2100) under four climatic scenarios (SSP126, SSP245, SSP370, SSP585).

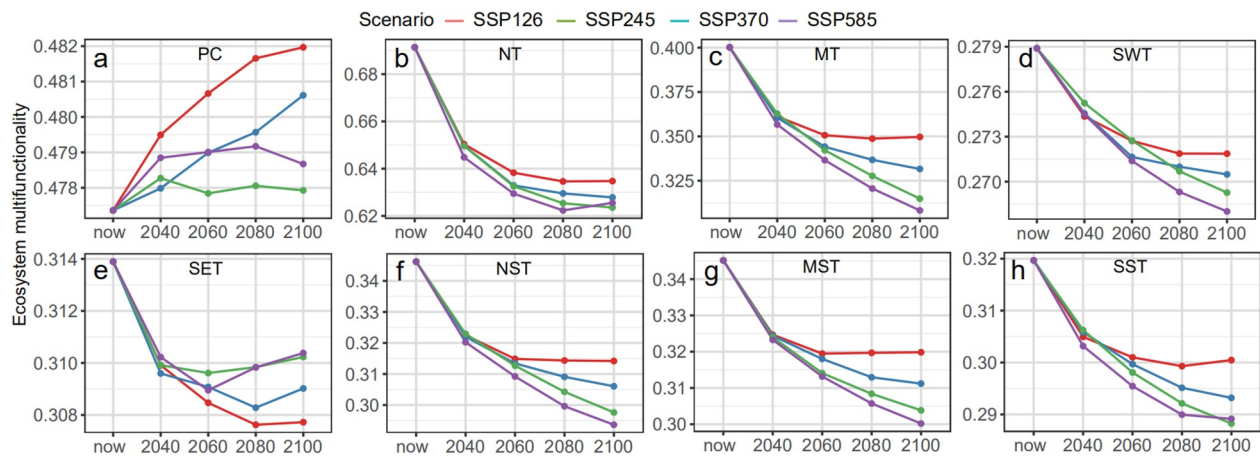


**Figure 6.** Dynamics of ecosystem multifunctionality in the climatic zones under different climatic scenarios. Each subplot shows temporal trends of EMF for: (a) Plateau climatic zone (PC). (b) Northern temperate zone (NT). (c) Mid-temperate zone (MT). (d) Southwestern temperate zone (SWT). (e) Southeastern temperate zone (SET). (f) Northern subtropical zone (NST). (g) Mid-subtropical zone (MST). (h) Southern subtropical zone (SST).

Figure 1 presented that EMF was higher in northeastern China and the southeastern Tibetan Plateau and lower in arid areas, suggesting the spatial heterogeneity of EMF. Another study indicated that EMF was generally high in cold areas but decreased with rising temperatures (Maestre et al., 2012). Warming can lead to increased surface-water evaporation and continuous soil drought (Dai et al., 2018), which will ultimately reduce biodiversity and affect ecosystem functions and services (Delgado-Baquerizo, Maestre, Eldridge, et al., 2016; Delgado-Baquerizo, Maestre, Reich, et al., 2016). The rate of material circulation, though, is slow in cold regions, which favors the accumulation of soil organic material (Lange et al., 2015; Schuur et al., 2015). Furthermore, EMF is also higher in alpine meadows than alpine steppes, possibly due to variations in precipitation (Song et al., 2020; Wang, Liu, et al., 2022; Wang, Sun, et al., 2022). Precipitation is higher in alpine meadows, contributing to increased species richness and improved ecosystem stability and sustainability (Delgado-Baquerizo et al., 2017; Maestre et al., 2012). The elevational pattern of EMF in our study revealed four distinct thresholds (582, 1,373, 3,726, and 5,477 m), showing more complex variation than the previous field study (3,900 m within a 3,030–5,000 m sampling elevation range, Wang et al., 2023). While the field study provided in situ observed data within their specific elevation band, our pixel-scale analysis encompassed the complete elevation gradient across diverse topographic positions. The incorporation of vegetation functional traits, notably leaf and root nutrient concentrations, enhanced EMF sensitivity to elevation-driven ecological changes. Altitude regulates the variations of climatic factors, hydrothermal patterns, and plant community composition (Pan et al., 2017). A study of an alpine transect with altitudinal gradients ranging from 3,813 to 4,807 m demonstrated that altitude and climate affect plant height, aboveground biomass, species richness, and the ratio of palatable species, and alter aboveground EMF. It is evident that harsh habitats in high-altitude areas (above 3,726 m), such as significant temperature differences and dry air, are not conducive to the survival of many organisms and lead to decreases in species richness. Conversely, the mild and humid climates in low-altitude regions (ranging from 1,373 to 3,726 m) foster high species richness and biological resources, consequently resulting in high ecosystem functions (Chen et al., 2022). This phenomenon defines that EMF and biodiversity are consistent with the hypothesis of the “mid-altitude bulge” along altitudinal gradients (Lomolino, 2001; Whittaker & Niering, 1975).

#### 4.2. Climate and Topography Determine the Spatial Pattern of EMF

EMF varied significantly ( $P < 0.001$ ) across the eight climatic zones (Figure 1c), indicating that changes in temperature and precipitation patterns could govern the spatial distribution of EMF. We therefore explored the mechanisms and drivers of EMF in different climatic zones. Our findings identified climate and topography as the key drivers of the spatial distribution of EMF (Figure 3). Furthermore, soil abiotic properties emerge as the dominant driver of EMF, surpassing the direct effects of bioclimate factors (Figure 3 and Figure S5 in Supporting Information S1) in PC. In detail, soil-mediated control likely stems from the unique ecological constraints of alpine ecosystems (Wang et al., 2021). The cold, nutrient-limited conditions in PC strongly suppress microbial decomposition rates and nutrient cycling, which results in soil biogeochemical properties acting a critical

bottleneck for alpine ecosystem function (C. Zhang et al., 2023; D. Zhang et al., 2023). Additionally, the relatively stable thermal and hydrological regimes in PC may enable soil properties to maintain a more sustained effect on ecosystem processes. Moreover, bioclimate factors primarily affect EMF by mediating soil abiotic properties, rather than through direct effects (Figure S5 in Supporting Information S1). Previous reports demonstrated that a warm-humid environment plays a key role in enhancing community carbon accumulation rates via modulating the availability of soil nutrients (soil available nitrogen, and soil available phosphorus) across the Tibetan Plateau (Sun et al., 2020). Furthermore, increased water and heat availability stimulates the activities of soil microorganisms, which indirectly promotes soil mineralization and potentially enhances plant resource utilization, thereby supporting the sustainability of EMF (Chen et al., 2018; Melillo et al., 2002).

Temperature harmed EMF in the temperate regions compared to PC, while precipitation promoted EMF (Figure 2). This is consistent with findings that warming can diminish relevant belowground ecosystem functions related to nutrient cycling, and soil fertility, and ultimately impair EMF, as demonstrated in dryland ecosystems (Hu et al., 2021). Biodiversity presented an inhibitory effect on EMF in NT and MT (Figure 3 and Figure S5 in Supporting Information S1), whereas a positive role was observed in a broad range of taxa and ecosystems (Lefcheck et al., 2015). In northern China, an unexpected negative correlation between soil microbial diversity and soil multifunctionality has been documented (Hu et al., 2021), consistent with findings in some natural ecosystems (Gamfeldt & Roger, 2017; Jing et al., 2020; van der Plas, 2019). One possible explanation is that increased microbial diversity could foster competition and suppress key species that are essential for nutrient cycling, thereby disturbing symbiotic microbial relationships (Delgado-Baquerizo, Maestre, Eldridge, et al., 2016; Delgado-Baquerizo, Maestre, Reich, et al., 2016; Delgado-Baquerizo et al., 2020). Under environmental stress, microbial species adapted to drought or low nutrient conditions may become dominant. This competitive exclusion leads to reduced overall diversity, yet key ecosystem functions can be maintained or even enhanced. Such disturbances are likely to inhibit plant growth and undermine soil multifunctionality. Moreover, land-use pressures can decouple the positive associations between plant richness and functions in the grasslands of northern China (Zhu et al., 2020).

Similarly, temperature also exerted an inhibitory effect on EMF in tropical regions (Figure 2). However, isothermality and the mean diurnal temperature range had a positive impact on EMF. Some studies have reported that within the suitable temperature range for vegetation growth, a greater diurnal temperature variation is associated with higher vegetation production (McCormick et al., 2006; Wan et al., 2009). Photosynthesis yields more organic matter during the day, and lower night-time temperatures reduce vegetation respiration, thereby increasing net nutrient accumulation (Fu et al., 2016; Peng et al., 2004; Piao et al., 2015). While most precipitation indicators decreased EMF, the seasonality of precipitation increased EMF in NST, MST, and SST. The reason is that different species are active at different growth periods, depending on seasonal rainfall patterns (e.g., wet and dry seasons). This temporal niche complementarity ensures that ecosystem functions are maintained across seasons. Moreover, although annual precipitation is higher in the tropics than in other regions, slight variations in precipitation can alter the water cycle, which can affect river flow and subsequently the ecosystem functions (Dubois et al., 2014; Potter et al., 2005). In the tropics, seasonal precipitation availability positively controls soil microbial respiration, leading to increased carbon storage and vegetation productivity (Feng et al., 2012; Rohr et al., 2013).

### 4.3. EMF Will Be Lost Rapidly on a Centurial Scale

It is anticipated that climatic changes and human pressure will escalate continuously until the end of the century, posing a threat to various ecosystems (Berdugo et al., 2020; Zscheischler et al., 2018). The rapid loss of EMF (Figures 4 and 5) is primarily driven by climate-induced ecosystem degradation (Allan et al., 2015; Birkhofer et al., 2018). Warming, altered precipitation regimes, and increased extreme climate events have reduced the resilience and function of ecosystems across multiple climatic zones (Tang et al., 2025). For instance, climate changes resulted in forest degradation, declined cropland productivity, and diminished carbon sequestration and soil fertility directly (Fernández-Martínez et al., 2019; Qiao et al., 2022). Under climate change, additional consideration of land-use changes (e.g., reduction in cropland and forest) may potentially exacerbate EMF loss (Figure S7 in Supporting Information S1), though the future impact of these changes remains uncertain (Bayer et al., 2023; Krause et al., 2019; Kuang et al., 2021). In addition, our projections assumed static soil properties, topography and biodiversity to isolate climate effects, but these factors will likely co-evolve with climate change. Soil organic matter may decline in intensively managed areas but increase in reforested regions, creating spatial heterogeneity in EMF responses (Liu et al., 2025; Van Rijssel et al., 2025). Similarly, species range shifts could

alter EMF patterns, with time lags in high-altitude ecosystems (Maestre et al., 2012; Xu et al., 2024). Given these complex and interacting dynamics, proactive management becomes essential.

Our projections indicate a gradual increase in EMF in PC across future scenarios (Figure 6). This trend can be attributed to several climate-mediated factors. Moderate warming extends the growing season and improves thermal conditions for vegetation (Yan et al., 2024). Furthermore, altered precipitation patterns may enhance water availability in historically arid areas (C. Zhang et al., 2023; D. Zhang et al., 2023). These combined hydrothermal changes are conducive to increased plant productivity and biomass accumulation, which in turn contribute significantly to enhanced ecosystem carbon sequestration (Sun et al., 2024). Despite these positive developments in PC, other climatic zones are experiencing EMF degradation, which requires urgent attention. Therefore, we propose several policy priorities to mitigate further EMF degradation. First, it is imperative that regional climate adaptation strategies should account for the varying vulnerabilities across climatic zones. This necessitates a particular focus on protecting the most vulnerable temperate zones while supporting the sustainable development pathways on the Tibetan Plateau. Second, EMF projections should be incorporated into regional land-use planning frameworks to guide conservation efforts in sensitive ecological areas (Scherzinger et al., 2024). Moreover, successfully mitigating EMF degradation requires coordinated, cross-sectoral policies (Sun, Fu, et al., 2021; Sun, Liang, et al., 2021). These policies must align ecological protection with sustainable development goals. Ultimately, these measures should be implemented within China's existing Ecological Conservation Redline framework to ensure their efficacy and institutional support.

## 5. Conclusions

Our comprehensive assessment of EMF in China reveals remarkable differences in EMF among different climatic zones and confirms that climate and topography are the primary drivers. Future projections indicate that more than 66% of EMF will experience degradation under different future climate scenarios at the end of this century. Especially, the rapid loss of EMF will be severe and long-lasting under high-emission scenarios. Our findings provide important insights into EMF patterns and dynamics, but several limitations should be noted. EMF assessment inherits uncertainties from indicator selection and integration approaches. Meanwhile, our predictions assume a stable relationship between climate and EMF, alongside static non-climatic factors. Future research should incorporate dynamic environment models and anthropogenic influences to better predict the response of EMF to global change. Despite these limitations, our study highlights the urgent need to maintain EMF to mitigate climate change.

## Conflict of Interest

The authors declare no conflicts of interest relevant to this study.

## Data Availability Statement

All underlying raw model data are publicly available online. Data for ecosystem functions such as SAN, SAP, STN, STP, and SOM are available in Shangguan and Dai (2021). SMBC, SMBN, and SMBP data are available in Gao et al. (2022). ABC and BBC data are available in Spawn and Gibbs (2020). VLN, VLP, VRN, VRP data are available in Zhang et al. (2021). Current bioclimatic data are available in Fick and Hijmans (2017). Future bioclimatic data are available at [https://www.worldclim.org/data/cmip6/cmip6\\_clim30s.html](https://www.worldclim.org/data/cmip6/cmip6_clim30s.html). DEM data are available in Jarvis et al. (2008). Soil bulk density, clay concentration, porosity and pH are available in Shangguan and Dai (2021). Soil moisture contents are available in Zhang et al. (2022). Biodiversity data are available in Sabatini et al. (2022). NPP data are available in Running and Zhao (2021). Analysis were executed using R open source software (R Core Team, 2020), Python software (Python Software Foundation, 2023) and CMP software (Gaucherel et al., 2018).

## References

- Abdi, H., & Williams, L. J. (2010). Principal component analysis. *Wiley Interdisciplinary Reviews: Computational Statistics*, 2(4), 433–459. <https://doi.org/10.1002/wics.101>
- Allan, E., Manning, P., Alt, F., Binkenstein, J., Blaser, S., Blüthgen, N., et al. (2015). Land use intensification alters ecosystem multifunctionality via loss of biodiversity and changes to functional composition. *Ecology Letters*, 18(8), 834–843. <https://doi.org/10.1111/ele.12469>
- An, H., Tang, Z., Keesstra, S., & Shangguan, Z. (2019). Impact of desertification on soil and plant nutrient stoichiometry in a desert grassland. *Scientific Reports*, 9(1), 9422. <https://doi.org/10.1038/s41598-019-45927-0>

## Acknowledgments

This research was supported by the Science and Technology Projects of Xizang Autonomous Region (XZ202501ZY0091); the Second Tibetan Plateau Scientific Expedition and Research (2019QZKK0405); the Joint Research Project of Three-River-Resource National Park Funded by the Chinese Academy of Sciences and Qinghai Provincial People's Government (LHZX-2020-08); the National Key Research and Development Program of China (2023YFE0121900); the National Natural Science Foundation of China (42377168); and MCIN, AEI/10.13039/501100011033 European Union Next Generation EU/PRTR (PID2022-140808NB-I00 and TED2021-132627-B-I00).

- Bayer, A. D., Lautenbach, S., & Arneth, A. (2023). Benefits and trade-offs of optimizing global land use for food, water, and carbon. *Proceedings of the National Academy of Sciences of the United States of America*, *120*(42), e2220371120. <https://doi.org/10.1073/pnas.2220371120>
- Berdugo, M., Delgado-Baquerizo, M., Soliveres, S., Hernández-Clemente, R., Zhao, Y., Gaitán, J. J., et al. (2020). Global ecosystem thresholds driven by aridity. *Science*, *367*(6479), 787–790. <https://doi.org/10.1126/science.aay5958>
- Birkhofer, K., Andersson, G. K. S., Bengtsson, J., Bommarco, R., Dänhardt, J., Ekbom, B., et al. (2018). Relationships between multiple biodiversity components and ecosystem services along a landscape complexity gradient. *Biological Conservation*, *218*, 247–253. <https://doi.org/10.1016/j.biocon.2017.12.027>
- Booker, D., & Snelder, T. (2012). Comparing methods for estimating flow duration curves at ungauged sites. *Journal of Hydrology*, *434*, 78–94. <https://doi.org/10.1016/j.jhydrol.2012.02.031>
- Both, S., Elias, D. M. O., Kritzler, U. H., Ostle, N. J., & Johnson, D. (2017). Land use not litter quality is a stronger driver of decomposition in hyperdiverse tropical forest. *Ecology and Evolution*, *7*(22), 9307–9318. <https://doi.org/10.1002/ece3.3460>
- Bovik, A. C. (2009). *Chapter 3—Basic gray level image processing (prevajalec, Trans.)*. V Bovik, A. (ur.), *the essential guide to image processing (str. 43-68)*. Academic Press. <https://doi.org/10.1016/B978-0-12-374457-9.00003-2>
- Bradford, M. A., Wood, S. A., Bardgett, R. D., Black, H. I., Bonkowski, M., Eggers, T., et al. (2014). Discontinuity in the responses of ecosystem processes and multifunctionality to altered soil community composition. *Proceedings of the National Academy of Sciences of the United States of America*, *111*(40), 14478–14483. <https://doi.org/10.1073/pnas.1413707111>
- Byrnes, J., Lefcheck, J. S., Gamfeldt, L., Griffin, J. N., Isbell, F., & Hector, A. (2014). Multifunctionality does not imply that all functions are positively correlated. *Proceedings of the National Academy of Sciences of the United States of America*, *111*(51), E5490. <https://doi.org/10.1073/pnas.1419515112>
- Cardinale, B. J., Duffy, J. E., Gonzalez, A., Hooper, D. U., Perrings, C., Venail, P., et al. (2012). Biodiversity loss and its impact on humanity. *Nature*, *486*(7401), 59–67. <https://doi.org/10.1038/nature11148>
- Carpenter, S. R., Mooney, H. A., Agard, J., Capistrano, D., DeFries, R. S., Diaz, S., et al. (2009). Science for managing ecosystem services: Beyond the millennium ecosystem assessment. *Proceedings of the National Academy of Sciences of the United States of America*, *106*(5), 1305–1312. <https://doi.org/10.1073/pnas.0808772106>
- Chen, L., Liu, L., Mao, C., Qin, S., Wang, J., Liu, F., et al. (2018). Nitrogen availability regulates topsoil carbon dynamics after permafrost thaw by altering microbial metabolic efficiency. *Nature Communications*, *9*(1), 3951. <https://doi.org/10.1038/s41467-018-06232-y>
- Chen, W., Wang, J., Chen, X., Meng, Z., Xu, R., Duoqi, D., et al. (2022). Soil microbial network complexity predicts ecosystem function along elevation gradients on the Tibetan Plateau. *Soil Biology and Biochemistry*, *172*, 108766. <https://doi.org/10.1016/j.soilbio.2022.108766>
- Cutler, D. R., Edwards, T. C., Jr., Beard, K. H., Cutler, A., Hess, K. T., Gibson, J., & Lawler, J. J. (2007). Random forests for classification in ecology. *Ecology*, *88*(11), 2783–2792. <https://doi.org/10.1890/07-0539.1>
- Dai, A., Zhao, T., & Chen, J. (2018). Climate change and drought: A precipitation and evaporation perspective. *Current Climate Change Reports*, *4*(3), 301–312. <https://doi.org/10.1007/s40641-018-0101-6>
- Delgado-Baquerizo, M., Maestre, F. T., Eldridge, D. J., Bowker, M. A., Ochoa, V., Gozalo, B., et al. (2016). Biocrust-forming mosses mitigate the negative impacts of increasing aridity on ecosystem multifunctionality in drylands. *New Phytologist*, *209*(4), 1540–1552. <https://doi.org/10.1111/nph.13688>
- Delgado-Baquerizo, M., Maestre, F. T., Reich, P. B., Jeffries, T. C., Gaitán, J. J., Encinar, D., et al. (2016). Microbial diversity drives multifunctionality in terrestrial ecosystems. *Nature Communications*, *7*(1), 10541. <https://doi.org/10.1038/ncomms10541>
- Delgado-Baquerizo, M., Reich, P. B., Trivedi, C., Eldridge, D. J., Abades, S., Alfaro, F. D., et al. (2020). Multiple elements of soil biodiversity drive ecosystem functions across biomes. *Nature Ecology & Evolution*, *4*(2), 210–220. <https://doi.org/10.1038/s41559-019-1084-y>
- Delgado-Baquerizo, M., Trivedi, P., Trivedi, C., Eldridge, D. J., Reich, P. B., Jeffries, T. C., et al. (2017). Microbial richness and composition independently drive soil multifunctionality. *Functional Ecology*, *31*(12), 2330–2343. <https://doi.org/10.1111/1365-2435.12924>
- Dooley, Á., Isbell, F., Kirwan, L., Connolly, J., Finn, J. A., & Brophy, C. (2015). Testing the effects of diversity on ecosystem multifunctionality using a multivariate model. *Ecology Letters*, *18*(11), 1242–1251. <https://doi.org/10.1111/ele.12504>
- Dubois, N., Oppo, D. W., Galy, V. V., Mohtadi, M., Van Der Kaars, S., Tierney, J. E., et al. (2014). Indonesian vegetation response to changes in rainfall seasonality over the past 25,000 years. *Nature Geoscience*, *7*(7), 513–517. <https://doi.org/10.1038/ngeo2182>
- Feng, X., Vico, G., & Porporato, A. (2012). On the effects of seasonality on soil water balance and plant growth. *Water Resources Research*, *48*(5), W05543. <https://doi.org/10.1029/2011WR011263>
- Fernández-Martínez, M., Sardans, J., Chevallier, F., Ciais, P., Obersteiner, M., Vicca, S., et al. (2019). Global trends in carbon sinks and their relationships with CO<sub>2</sub> and temperature. *Nature Climate Change*, *9*(1), 73–79. <https://doi.org/10.1038/s41558-018-0367-7>
- Fick, S. E., & Hijmans, R. J. (2017). WorldClim 2: New 1km spatial resolution climate surfaces for global land areas [Dataset]. *Worldclim*. Retrieved from <https://www.worldclim.org/data/worldclim21.html>
- Field, C. B., Behrenfeld, M. J., Randerson, J. T., & Falkowski, P. (1998). Primary production of the biosphere: Integrating terrestrial and oceanic components. *Science*, *281*(5374), 237–240. <https://doi.org/10.1126/science.281.5374.237>
- Fry, E. L., Manning, P., Macdonald, C., Hasegawa, S., De Palma, A., Power, S. A., & Singh, B. K. (2016). Shifts in microbial communities do not explain the response of grassland ecosystem function to plant functional composition and rainfall change. *Soil Biology and Biochemistry*, *92*, 199–210. <https://doi.org/10.1016/j.soilbio.2015.10.006>
- Fu, Y. H., Liu, Y., De Boeck, H. J., Menzel, A., Nijs, I., Peaucelle, M., et al. (2016). Three times greater weight of daytime than of night-time temperature on leaf unfolding phenology in temperate trees. *New Phytologist*, *212*(3), 590–597. <https://doi.org/10.1111/nph.14073>
- Gamfeldt, L., Hillebrand, H., & Jonsson, P. R. (2008). Multiple functions increase the importance of biodiversity for overall ecosystem functioning. *Ecology*, *89*(5), 1223–1231. <https://doi.org/10.1890/06-2091.1>
- Gamfeldt, L., & Roger, F. (2017). Revisiting the biodiversity-ecosystem multifunctionality relationship. *Nature Ecology & Evolution*, *1*(7), 0168. <https://doi.org/10.1038/s41559-017-0168>
- Gao, D., Bai, E., Wang, S., Zong, S., Liu, Z., Fan, X., et al. (2022). Three-dimensional mapping of carbon, nitrogen, and phosphorus in soil microbial biomass and their stoichiometry at the global scale [Dataset]. *Zenodo*. <https://doi.org/10.5281/zenodo.6950624>
- García, R. A., Cabeza, M., Rahbek, C., & Araújo, M. B. (2014). Multiple dimensions of climate change and their implications for biodiversity. *Science*, *344*(6183), 1247579. <https://doi.org/10.1126/science.1247579>
- Garland, G., Banerjee, S., Edlinger, A., Miranda Oliveira, E., Herzog, C., Wittwer, R., et al. (2021). A closer look at the functions behind ecosystem multifunctionality: A review. *Journal of Ecology*, *109*(2), 600–613. <https://doi.org/10.1111/1365-2745.13511>
- Gaucherel, C., Alleaume, S., & Hély, C. (2008). The comparison map profile method: A strategy for multiscale comparison of quantitative and qualitative images. *IEEE Transactions on Geoscience and Remote Sensing*, *46*(9), 2708–2719. <https://doi.org/10.1109/TGRS.2008.919379>
- Gaucherel, C., Tramier, C., Devictor, V., Svenning, J. C., & Hély, C. (2018). Where and at which scales does the latitudinal diversity gradient fail? [Software]. *Journal of Biogeography*, *45*(8), 1905–1916. <https://doi.org/10.1111/jbi.13355>

- He, W., Ye, C., Sun, J., Xiong, J., Wang, J., & Zhou, T. (2020). Dynamics and drivers of the alpine timberline on Gongga Mountain of Tibetan Plateau-adopted from the Otsu method on google Earth engine. *Remote Sensing*, *12*(16), 2651. <https://doi.org/10.3390/rs12162651>
- Hector, A., & Bagchi, R. (2007). Biodiversity and ecosystem multifunctionality. *Nature*, *448*(7150), 188–190. <https://doi.org/10.1038/nature05947>
- Hu, W., Ran, J., Dong, L., Du, Q., Ji, M., Yao, S., et al. (2021). Aridity-driven shift in biodiversity–soil multifunctionality relationships. *Nature Communications*, *12*(1), 5350. <https://doi.org/10.1038/s41467-021-25641-0>
- Isbell, F., Calcagno, V., Hector, A., Connolly, J., Harpole, W. S., Reich, P. B., et al. (2011). High plant diversity is needed to maintain ecosystem services. *Nature*, *477*(7363), 199–202. <https://doi.org/10.1038/nature10282>
- Jarvis, A., Reuter, H. I., Nelson, A., & Guevara, E. (2008). Hole-filled seamless SRTM data V4 [Dataset]. *International Centre for Tropical Agriculture (CIAT)*. Retrieved from <https://srtm.csi.cgiar.org>
- Jing, X., Prager, C. M., Classen, A. T., Maestre, F. T., He, J. S., & Sanders, N. J. (2020). Variation in the methods leads to variation in the interpretation of biodiversity-ecosystem multifunctionality relationships. *Journal of Plant Ecology*, *13*(4), 431–441. <https://doi.org/10.1093/jpe/rtaa031>
- Jing, X., Sanders, N. J., Shi, Y., Chu, H., Classen, A. T., Zhao, K., et al. (2015). The links between ecosystem multifunctionality and above-and belowground biodiversity are mediated by climate. *Nature Communications*, *6*(1), 8159. <https://doi.org/10.1038/ncomms9159>
- Krause, A., Haverd, V., Poulter, B., Anthoni, P., Quesada, B., Rammig, A., & Arnett, A. (2019). Multimodel analysis of future land use and climate change impacts on ecosystem functioning. *Earth's Future*, *7*(7), 833–851. <https://doi.org/10.1029/2018EF001123>
- Kruskal, W. H., & Wallis, W. A. (1952). Use of ranks in one-criterion variance analysis. *Journal of the American Statistical Association*, *47*(260), 583–621. <https://doi.org/10.1080/01621459.1952.10483441>
- Kuang, W., Liu, J., Tian, H., Shi, H., Dong, J., Song, C., et al. (2021). Cropland redistribution to marginal lands undermines environmental sustainability. *National Science Review*, *9*(1), nwab091. <https://doi.org/10.1093/nsr/nwab091>
- Lange, M., Eisenhauer, N., Sierra, C. A., Bessler, H., Engels, C., Griffiths, R. I., et al. (2015). Plant diversity increases soil microbial activity and soil carbon storage. *Nature Communications*, *6*(1), 6707. <https://doi.org/10.1038/ncomms7707>
- Lavelle, S., & Grigulis, K. (2012). How fundamental plant functional trait relationships scale-up to trade-offs and synergies in ecosystem services. *Journal of Ecology*, *100*(1), 128–140. <https://doi.org/10.1111/j.1365-2745.2011.01914.x>
- Lefcheck, J. S., Byrnes, J. E., Isbell, F., Gamfeldt, L., Griffin, J. N., Eisenhauer, N., et al. (2015). Biodiversity enhances ecosystem multifunctionality across trophic levels and habitats. *Nature Communications*, *6*(1), 6936. <https://doi.org/10.1038/ncomms7936>
- Li, X., He, Y., Zeng, Z., Lian, X., Wang, X., Du, M., et al. (2018). Spatiotemporal pattern of terrestrial evapotranspiration in China during the past thirty years. *Agricultural and Forest Meteorology*, *259*, 131–140. <https://doi.org/10.1016/j.agrformet.2018.04.020>
- Liu, T., Yu, L., Chen, J., Qi, W., Wu, H., Peng, D., et al. (2025). Afforestation surpasses abandonment in the recovery of post-agricultural soil organic carbon in China as estimated by machine learning models. *Global Change Biology*, *31*(8), e70383. <https://doi.org/10.1111/gcb.70383>
- Lomolino, M. V. (2001). Elevation gradients of species-density: Historical and prospective views. *Global Ecology and Biogeography*, *10*(1), 3–13. <https://doi.org/10.1046/j.1466-822x.2001.00229.x>
- Maestre, F. T., Quero, J. L., Gotelli, N. J., Escudero, A., Ochoa, V., Delgado-Baquerizo, M., et al. (2012). Plant species richness and ecosystem multifunctionality in global drylands. *Science*, *335*(6065), 214–218. <https://doi.org/10.1126/science.1215442>
- Manning, P., van der Plas, F., Soliveres, S., Allan, E., Maestre, F. T., Mace, G., et al. (2018). Redefining ecosystem multifunctionality. *Nature Ecology & Evolution*, *2*(3), 427–436. <https://doi.org/10.1038/s41559-017-0461-7>
- Masson-Delmotte, V., Zhai, P., Pirani, A., Connors, S. L., Péan, C., Berger, S., et al. (2021). Climate change 2021: The physical science basis. In *Contribution of Working Group I to the Sixth Assessment Report of the Intergovernmental Panel on Climate Change* (Vol. 2). Retrieved from <https://www.ipcc.ch/report/ar6/wg1/>
- Mastrangelo, M. E., Weyland, F., Villarino, S. H., Barral, M. P., Nahuelhual, L., & Littera, P. (2014). Concepts and methods for landscape multifunctionality and a unifying framework based on ecosystem services. *Landscape Ecology*, *29*(2), 345–358. <https://doi.org/10.1007/s10980-013-9959-9>
- McCormick, A., Cramer, M., & Watt, D. (2006). Sink strength regulates photosynthesis in sugarcane. *New Phytologist*, *171*(4), 759–770. <https://doi.org/10.1111/j.1469-8137.2006.01785.x>
- Melillo, J. M., Steudler, P. A., Aber, J. D., Newkirk, K., Lux, H., Bowles, F. P., et al. (2002). Soil warming and carbon-cycle feedbacks to the climate system. *Science*, *298*(5601), 2173–2176. <https://doi.org/10.1126/science.1074153>
- Meyer, S. T., Ptacnik, R., Hillebrand, H., Bessler, H., Buchmann, N., Ebeling, A., et al. (2018). Biodiversity–multifunctionality relationships depend on identity and number of measured functions. *Nature Ecology & Evolution*, *2*(1), 44–49. <https://doi.org/10.1038/s41559-017-0391-4>
- Oliver, T. H., Heard, M. S., Isaac, N. J., Roy, D. B., Procter, D., Eigenbrod, F., et al. (2015). Biodiversity and resilience of ecosystem functions. *Trends in Ecology & Evolution*, *30*(11), 673–684. <https://doi.org/10.1016/j.tree.2015.08.009>
- Pan, Y., Wu, J.-X., Luo, L.-M., Tu, Y.-L., Yu, C.-Q., Zhang, X.-Z., et al. (2017). Climatic and geographic factors affect ecosystem multifunctionality through biodiversity in the Tibetan alpine grasslands. *Journal of Mountain Science*, *14*(8), 1604–1614. <https://doi.org/10.1007/s11629-016-4242-6>
- Peng, S., Huang, J., Sheehy, J. E., Laza, R. C., Visperas, R. M., Zhong, X., et al. (2004). Rice yields decline with higher night temperature from global warming. *Proceedings of the National Academy of Sciences of the United States of America*, *101*(27), 9971–9975. <https://doi.org/10.1073/pnas.0403720101>
- Piao, S., Tan, J., Chen, A., Fu, Y. H., Ciais, P., Liu, Q., et al. (2015). Leaf onset in the northern hemisphere triggered by daytime temperature. *Nature Communications*, *6*(1), 6911. <https://doi.org/10.1038/ncomms7911>
- Potter, N., Zhang, L., Milly, P., McMahon, T. A., & Jakeman, A. (2005). Effects of rainfall seasonality and soil moisture capacity on mean annual water balance for Australian catchments. *Water Resources Research*, *41*(6), W06007. <https://doi.org/10.1029/2004WR003697>
- Python Software Foundation. (2023). Python: A programming language for general-purpose programming (version 3.13.5) [Software]. *Python Software Foundation*. Retrieved from <https://www.python.org/>
- Qiao, L., Wang, X., Smith, P., Fan, J., Lu, Y., Emmett, B., et al. (2022). Soil quality both increases crop production and improves resilience to climate change. *Nature Climate Change*, *12*(6), 574–580. <https://doi.org/10.1038/s41558-022-01376-8>
- R Core Team. (2020). R: A language and environment for statistical computing (4.0.0) [Software]. *R Foundation for Statistical Computing*. Retrieved from <https://www.R-project.org/>
- Riahi, K., Van Vuuren, D. P., Kriegler, E., Edmonds, J., O'Neill, B. C., Fujimori, S., et al. (2017). The shared socioeconomic pathways and their energy, land use, and greenhouse gas emissions implications: An overview. *Global Environmental Change*, *42*, 153–168. <https://doi.org/10.1016/j.gloenvcha.2016.05.009>
- Rohr, T., Manzoni, S., Feng, X., Menezes, R. S., & Porporato, A. (2013). Effect of rainfall seasonality on carbon storage in tropical dry ecosystems. *Journal of Geophysical Research: Biogeosciences*, *118*(3), 1156–1167. <https://doi.org/10.1002/jgrg.20091>

- Running, S., & Zhao, M. (2021). MODIS/terra net primary production gap-filled yearly L4 global 500m SIN grid V061 [Dataset]. *NASA Land Processes Distributed Active Archive Center*. <https://doi.org/10.5067/MODIS/MOD17A3HGF.061>
- Sabatini, F. M., Jiménez-Alfaro, B., Jandt, U., Chytrý, M., Bruehlheide, H., & Consortium, t. s. (2022). Global patterns of vascular plant alpha-diversity [Dataset]. *iDiv Data Repository*. <https://doi.org/10.25829/ividiv.3506-p4c0mo>
- Scherzinger, F., Schädler, M., Reitz, T., Yin, R., Auge, H., Merbach, I., et al. (2024). Sustainable land management enhances ecological and economic multifunctionality under ambient and future climate. *Nature Communications*, *15*(1), 4930. <https://doi.org/10.1038/s41467-024-48830-z>
- Schuur, E. A., McGuire, A. D., Schädel, C., Grosse, G., Harden, J. W., Hayes, D. J., et al. (2015). Climate change and the permafrost carbon feedback. *Nature*, *520*(7546), 171–179. <https://doi.org/10.1038/nature14338>
- Shangguan, W., & Dai, Y. (2021). A China dataset of soil properties for land surface modeling [Dataset]. *National Tibetan Plateau Data Center*. Retrieved from <https://data.tpdc.ac.cn/en/data/11573187-fd64-47b1-81a6-0c7c224112a0>
- Song, M. H., Zhu, J. F., Li, Y. K., Zhou, H. K., Xu, X. L., Cao, G. M., et al. (2020). Shifts in functional compositions predict desired multifunctionality along fragmentation intensities in an alpine grassland. *Ecological Indicators*, *112*, 106095. <https://doi.org/10.1016/j.ecolind.2020.106095>
- Spawn, S. A., & Gibbs, H. K. (2020). Global aboveground and belowground biomass carbon density maps for the year 2010 [Dataset]. *ORNL Distributed Active Archive Center*. <https://doi.org/10.3334/ORNLDAAAC/1763>
- Sun, J., Fu, B., Zhao, W., Liu, S., Liu, G., Zhou, H., et al. (2021). Optimizing grazing exclusion practices to achieve Goal 15 of the sustainable development goals in the Tibetan Plateau. *Science Bulletin*, *66*(15), 1493–1496. <https://doi.org/10.1016/j.scib.2021.03.014>
- Sun, J., Liang, E., Barrio, I. C., Chen, J., Wang, J., & Fu, B. (2021). Fences undermine biodiversity targets. *Science*, *374*(6565), 269. <https://doi.org/10.1126/science.abm3642>
- Sun, J., Wang, Y., Lee, T. M., Nie, X., Wang, T., Liang, E., et al. (2024). Nature-based Solutions can help restore degraded grasslands and increase carbon sequestration in the Tibetan Plateau. *Communications Earth & Environment*, *5*(1), 154. <https://doi.org/10.1038/s43247-024-01330-w>
- Sun, J., Zhou, T. C., Liu, M., Chen, Y. C., Liu, G. H., Xu, M., et al. (2020). Water and heat availability are drivers of the aboveground plant carbon accumulation rate in alpine grasslands on the Tibetan Plateau. *Global Ecology and Biogeography*, *29*(1), 50–64. <https://doi.org/10.1111/geb.13006>
- Tang, Y., Luo, M., Wu, S., & Li, X. (2025). Increasing synchrony of extreme heat and precipitation events under climate warming. *Geophysical Research Letters*, *52*(8), e2024GL113021. <https://doi.org/10.1029/2024GL113021>
- van der Plas, F. (2019). Biodiversity and ecosystem functioning in naturally assembled communities. *Biological Reviews*, *94*(4), 1220–1245. <https://doi.org/10.1111/brv.12499>
- van der Plas, F., Manning, P., Allan, E., Scherer-Lorenzen, M., Verheyen, K., Wirth, C., et al. (2016). Jack-of-all-trades effects drive biodiversity–ecosystem multifunctionality relationships in European forests. *Nature Communications*, *7*(1), 11109. <https://doi.org/10.1038/ncomms11109>
- van Rijssel, S. Q., Koorneef, G. J., Veen, G. F., Pulleman, M. M., de Goede, R. G. M., Comans, R. N. J., et al. (2025). Conventional and organic farms with more intensive management have lower soil functionality. *Science*, *388*(6745), 410–415. <https://doi.org/10.1126/science.adr0211>
- Wagg, C., Bender, S. F., Widmer, F., & Van Der Heijden, M. G. (2014). Soil biodiversity and soil community composition determine ecosystem multifunctionality. *Proceedings of the National Academy of Sciences of the United States of America*, *111*(14), 5266–5270. <https://doi.org/10.1073/pnas.1320054111>
- Wan, S., Xia, J., Liu, W., & Niu, S. (2009). Photosynthetic overcompensation under nocturnal warming enhances grassland carbon sequestration. *Ecology*, *90*(10), 2700–2710. <https://doi.org/10.1890/08-2026.1>
- Wang, Y., Liu, B., Zhao, J., Ye, C., Wei, L., Sun, J., et al. (2022). Global patterns and abiotic drivers of ecosystem multifunctionality in dominant natural ecosystems. *Environment International*, *168*, 107480. <https://doi.org/10.1016/j.envint.2022.107480>
- Wang, Y., Sun, J., He, W., Ye, C., Liu, B., Chen, Y., et al. (2022). Migration of vegetation boundary between alpine steppe and meadow on a century-scale across the Tibetan Plateau. *Ecological Indicators*, *136*, 108599. <https://doi.org/10.1016/j.ecolind.2022.108599>
- Wang, Y., Sun, J., & Lee, T. M. (2023). Altitude dependence of alpine grassland ecosystem multifunctionality across the Tibetan Plateau. *Journal of Environmental Management*, *332*, 117358. <https://doi.org/10.1016/j.jenvman.2023.117358>
- Wang, Y., Xiao, J., Ma, Y., Luo, Y., Hu, Z., Li, F., et al. (2021). Carbon fluxes and environmental controls across different alpine grassland types on the Tibetan Plateau. *Agricultural and Forest Meteorology*, *311*, 108694. <https://doi.org/10.1016/j.agrformet.2021.108694>
- Whittaker, R. H., & Niering, W. A. (1975). Vegetation of the Santa Catalina Mountains, Arizona. V. Biomass, production, and diversity along the elevation gradient. *Ecology*, *56*(4), 771–790. <https://doi.org/10.2307/1936291>
- Xu, Y., Dong, S., Gao, X., Yang, M., Li, S., Shen, H., et al. (2021). Aboveground community composition and soil moisture play determining roles in restoring ecosystem multifunctionality of alpine steppe on Qinghai-Tibetan Plateau. *Agriculture, Ecosystems & Environment*, *305*, 107163. <https://doi.org/10.1016/j.agee.2020.107163>
- Xu, Z., Guo, X., Allen, W. J., Yu, X., Hu, Y., Wang, J., et al. (2024). Plant community diversity alters the response of ecosystem multifunctionality to multiple global change factors. *Global Change Biology*, *30*(2), e17182. <https://doi.org/10.1111/gcb.17182>
- Yan, Z., Wang, T., Ding, J., Wang, X., Fu, Y. H., Li, J., et al. (2024). No slowdown of growing season extension with warming in a permafrost-affected meadow on the Tibetan Plateau. *Journal of Ecology*, *112*(8), 1774–1786. <https://doi.org/10.1111/1365-2745.14359>
- Zavaleta, E. S., Pasari, J. R., Hulvey, K. B., & Tilman, G. D. (2010). Sustaining multiple ecosystem functions in grassland communities requires higher biodiversity. *Proceedings of the National Academy of Sciences of the United States of America*, *107*(4), 1443–1446. <https://doi.org/10.1073/pnas.0906829107>
- Zhang, C., Long, D., Liu, T., Slater, L. J., Wang, G., Zuo, D., et al. (2023). Grassland greening and water resource availability may coexist in a warming climate in northern China and the Tibetan Plateau. *Earth's Future*, *11*(12), e2023EF004037. <https://doi.org/10.1029/2023EF004037>
- Zhang, D., Wang, L., Qin, S., Kou, D., Wang, S., Zheng, Z., et al. (2023). Microbial nitrogen and phosphorus co-limitation across permafrost region. *Global Change Biology*, *29*(14), 3910–3923. <https://doi.org/10.1111/gcb.16743>
- Zhang, Y., Guo, Y., Tang, Z., Feng, Y., Zhu, X., Xu, W., et al. (2021). Patterns of nitrogen and phosphorus pools in terrestrial ecosystems in China [Dataset]. *Dryad*. <https://doi.org/10.5061/dryad.6hdr7sqzx>
- Zhang, Y., Liang, S., Ma, H., He, T., Wang, Q., & Li, B. (2022). A global 1-km surface soil moisture product from 2000 to 2020 [Dataset]. *Zenodo*. <https://doi.org/10.5281/zenodo.7172664>
- Zhou, T., Sun, J., Ye, C., Jing, X., Liang, E., Lu, X., et al. (2025). Climate change is predicted to reduce global belowground ecosystem multifunctionality. *Nature Communications*, *16*(1), 9337. <https://doi.org/10.1038/s41467-025-64453-4>
- Zhu, Y., Delgado-Baquerizo, M., Shan, D., Yang, X., Liu, Y., & Eldridge, D. J. (2020). Diversity-productivity relationships vary in response to increasing land-use intensity. *Plant and Soil*, *450*(1), 511–520. <https://doi.org/10.1007/s11104-020-04516-1>
- Zirbel, C. R., Grman, E., Bassett, T., & Brudvig, L. A. (2019). Landscape context explains ecosystem multifunctionality in restored grasslands better than plant diversity. *Ecology*, *100*(4), e02634. <https://doi.org/10.1002/ecy.2634>
- Zscheischler, J., Westra, S., Van Den Hurk, B. J., Seneviratne, S. I., Ward, P. J., Pitman, A., et al. (2018). Future climate risk from compound events. *Nature Climate Change*, *8*(6), 469–477. <https://doi.org/10.1038/s41558-018-0156-3>